Received: 25 July 2018 | Accepted: 24 September 2018
DOI: 10.1002/stc.2282

RESEARCH ARTICLE

WILEY

Algorithms to determine wheel loads and speed of trains using strains measured on bridge girders

Thattarath Madathil Deepthi | Umakanthan Saravanan | Anumolu Meher Prasad

Department of Civil Engineering, Indian Institute of Technology Madras, India

Correspondence
Umakanthan Saravanan, Department of Civil Engineering, Indian Institute of Technology Madras, Chennai 600036, Tamil Nadu, India.
Email: saran@iitm.ac.in

Funding information
National Program on Micro and Smart Systems, Grant/Award Number: PARC 3.18

Summary

This paper reports a bridge weigh-in-motion system, for railways, when dynamic analysis is not required to determine the displacement response of the structure with reasonable accuracy. It is also assumed that the mechanism of resisting the axle loads is through bending action and the loads transferred to the bridge girder can be assumed to be point loads, as in the case of bridge without ballast. Because, the electric locomotive wheel load would be nearly constant and different from the wagon wheel load, except in case of a fully loaded freight train, the location of the locomotive and wagon can be identified from the time history of the measured shear strains. Further, whether a passing train is freight or passenger can be determined using the fact that the passenger trains arrive at close to scheduled times. Thus, using this information on the type of train and the arrangement of locomotive and wagons the distance between the wheel loads is determined. Estimate of the wheel speed and the load is done using two mechanics based algorithms. One of the algorithms is based on only the shear strain. Another algorithm uses shear strain to estimate the wheel speed and the axial strain to estimate the wheel load. The theoretical advantages and disadvantages of these algorithms are presented. Then, both the algorithms are bench marked with field data and their merits and demerits with respect to field implementation also documented.

KEYWORDS
axial strain, bridge weigh-in-motion, quasi-static, railway bridges, shear strain

1 | INTRODUCTION

Continuous monitoring of bridges is gaining popularity through out the world. This continuous monitoring of bridges, apart from indicating the current health of the bridge, could also be used to rationalize the design loads. Recorded strain time histories on the monitored bridge over a long period of time (say 6–12 months) could be used to estimate the actual wheel loads, speed, stress cycles, and the dynamic amplification factor for the instrumented structure. The loads specified as standard loads, are the maximum allowable loads. This standard value does not vary for electrical locomotive. However, for wagons, it varies depending on the weight of passengers or freight it hauls. Hence, the weight estimated from the field measured data will give an estimate of the actual loads that traverse the bridge. By fitting a probability density function (PDF) for these estimated quantities one can rationalize the design loads. Further, the probability of any future estimate of the response belonging to an above-determined PDF can be ascertained and used as an indicator of the health of the bridge. As pointed out in,[1] reliable information on traffic load data can also be used to support infrastructure management.

With this as the background, a fully automated and robust algorithm for estimating the wheel loads and speed from strain measurements is sought. Such systems are called the bridge weigh-in-motion (BWIM) in the literature. Several researchers in the past have used bending moment, acceleration, and deflection data to determine the equivalent static loads on highway bridges.[2-6] These studies have shown that estimation of wheel loads using strains give better results compared with those with acceleration and deflection. Weigh-in-motion studies on highway bridges can now be applied to most types of road bridges, as long as the effective influence lines used for weighing are shorter than 40 m.[7]

Even though development of BWIM for railway bridges is simpler than highway bridges, such studies have not been reported till Karoumi et al.[8] implemented one such system in a Swedish single span bridge. Methods like SUPERTRACK and FADLESS use pressure cells below, the track and strain gauges on the rails to estimate the axle loads.[9] In these studies, the wheel load estimation is done by minimizing the error between the theoretically estimated strain for a given wheel load and that observed experimentally. Minimization is done by optimization, employing either gradient based methods or nongradient based methods like the genetic algorithm. The influence lines developed using the responses of the known weights over the bridge or analytically is used to estimate the theoretical strains for given wheel loads. In this study, influence lines are developed analytically using the Müller-Breslau's principle[10] and calibrated using an electric locomotive with known wheel load moving over the bridge. Algorithms not based on optimization technique, utilizing the shear or axial strain time history, to find the wheel load, and speed is proposed.

In this study, contrary to the conventional BWIM system, the wheel loads are estimated by inversion of a single matrix. For the algorithm based on shear strain time history, the wheel loads are determined by inverting a sparse $q \times q$ matrix, where q is the number of wheel loads to be determined. In case of the algorithm based on axial strain, it is observed that the axial strain measured at a given time instant is a linear function of q unknown wheel loads. Hence, if the axial strain is measured at n time instances, the value of these q unknown wheel loads that best satisfies these n linear equations in the least squares sense is the pseudo inverse of the n by q sparse matrix. Typically, the number of measurement time instances is much larger than the number of unknown wheel loads.

Further, in conventional axial strain based BWIM, it is observed that the appropriateness of the estimated wheel speed determines the accuracy of the computed wheel loads. In most of the BWIM systems, the acceleration of the wheel due to the movement of the train is not considered. This might be appropriate for highway bridges wherein the time taken by the vehicle to pass a measurement point is small (less than a second). However, in case of railway bridges, the time taken by a typical train (500 m long) to cross a measurement point would be a few seconds (15 s). When the bridge is near a station or if there is a speed restriction upstream of the bridge, as in the case of the reported field study, trains crossing the bridge would not be at constant speed. Hence, assuming constant speed for a few second duration in case of railway bridges seems to be inappropriate, as observed from the field data and also pointed out by.[11,12] The algorithms reported in the literature for railway bridges[11,12] to measure speed is based on strain time history obtained at two points, as used in case of highway bridges. In this study, advantage is taken of the length of the train and the speed is estimated using the strain time history from a single point of measurement. This minimizes issues with time synchronous data acquisition and the required number of sensors. Further, the algorithm proposed here accounts for the speed to be any function of time; in particular, it allows for variable acceleration also. Nevertheless, it is specific enough to include constant speed also.

Hence, the objective of this paper is to present mechanics based algorithms to determine the wheel loads and speed of the trains, using the strain data at specific locations on the bridge. However, here it is assumed that the inertial forces are not significant to necessitate dynamic analysis of the problem. Also, the algorithms are developed and applied for bridges without ballast wherein the loads transferred to the bridge girder from the sleeper can be assumed as point loads. The applicability and effectiveness of the developed algorithms with respect to ballasted bridges needs study.

The organization of the paper is as follows. The algorithm for finding the train speed is presented in Section 2 and that for estimating the wheel load in Section 3. Working of the algorithms is illustrated using the field strain data from a steel plate girder bridge in Section 4. Validation of the results from the algorithm is presented in Section 5. A discussion on the field issues in the implementation of the algorithms is presented in Section 6. The article concludes with a summary of the salient observations and findings.

2 | ESTIMATION OF WHEEL SPEED

Existing algorithms to determine the speed requires strain time history measured at two points. They utilize the time at which the peak strain occurs to estimate the speed.

Here, the shear strain time history obtained at a single measurement point alone is utilized. Use is made of the fact that a local maximum of the shear strain occurs whenever a wheel load is at half the distance between the sleepers from the measurement point.[10] Thus, typically there would be as many peaks in the shear strain as the number of axles. Hence, from the shear strain time history, the local maximum shear strains and the time at which these occur are determined. Also, it is more easy to determine the peaks from the shear strains than the peaks of the axial strain because when the load crosses the section point of measurement, its contribution to the shear strain at the measurement point changes from being additive to subtractive, whereas the wheel loads contribution to the axial strain is always additive.[10]

By comparing the peak shear strain values, the configuration of the train (i.e., the number of locomotives and wagons, and also the position of each of them) can be obtained for all trains except for fully loaded freight trains. The mean of all the peak shear strains is determined as ϵ^s_{mean}. When the value of peak shear strain is significantly more than ϵ^s_{mean}, these peaks are caused due to locomotive wheels. Having identified the peak shear strains caused by the locomotive, the rest of the peaks are due to wagon wheels. However, for a fully loaded freight train, because the strain induced by both locomotive and fully loaded wagon are comparable, distinction between a locomotive induced strain and wagon induced strain is difficult. Generally, a fully loaded freight train configuration consists of two locomotives at the beginning, then followed with wagons. Hence, such a configuration is assumed for fully loaded freight trains. Using the above logic, the number of locomotives and wagons and their position is identified. Erroneous determination of the configuration of the train would result in the mismatch of the predicted and the observed strain time history. In such cases, the configuration of the train can be determined by trial and error procedure to one which results in the best agreement between the predicted and the observed strain time history.

The so determined configuration of the train is used to find the relative position of the wheel loads from the first wheel load. It is known that the location of the wheel loads depends on the type of electric locomotive and wagon. The type of electric locomotive and wagon depends on the class of train—long distance passenger, local passenger, or freight. Because the passenger trains always arrive within a fixed time interval and their shear strain signatures are nearly fixed (configuration of the passenger trains are fixed) and different from a freight train, they can be identified. Trains that are not passenger trains are taken as freight trains. Once the class of the train gets fixed, the location of the wheel loads can be determined because the distance of the wheel loads in the electric locomotive and wagon are standardized. Let the so determined position of each of the wheel loads from the first load be $\{\mathbf{s}\}$.

Let the time at which these peak strains occurred with the time of occurrence of the first peak taken as zero be $\{\mathbf{t}\}$. The time of occurrence of a wheel load at the measurement point, t is related to the distance from the first wheel load, s using a polynomial function of the form,

$$s = a_1 t + a_2 t^2 + a_3 t^3 + a_4 t^4 + \ ..., \tag{1}$$

where a_i's are constants. The constants a_i's for a given order polynomial are found so as to minimize the error,

$$\delta = \sum_{i=1}^{q} [s_i - (a_1 t_i + a_2 t_i^2 + a_3 t_i^3 + a_4 t_i^4)]^2, \tag{2}$$

where q is the number of wheel loads. The order of the polynomial is increased from 1 to such a value for which the adjusted R^2 value of the fit is greater than 0.99. The maximum order of the polynomial required in this study is four, which would typically be for long trains. However, for single locomotives and very short trains, first order polynomial is used.

Differentiating Equation (1) with respect to t yields speed of the train as a function of time.

3 | ESTIMATION OF WHEEL LOADS

Two methods to estimate the wheel loads from the strain data are explained in this section. One method utilizes the whole time series of the axial strain, and the second method is based on the peak values of the shear strain. Whereas axial strain based method requires a correct estimate of the position of the wheel loads at a given time instance, the shear strain method is independent of the determined wheel load positions as a function of time.

The wheel loads are assumed to be point forces at known distances between them, as determined in the previous section. The magnitude of these wheel loads is obtained so that the time history of the measured strain component agrees with that obtained theoretically using the influence line method. The coefficients in the influence line method

are computed theoretically using the Müller-Breslau's principle[10] in terms of the flexural or shear flexibility of the bridge. Using the time history of the axial and shear strains obtained when an electric locomotive with known wheel loads passes over the bridge, the flexural and shear flexibilities of the bridge is calibrated so that the wheel load determined from the algorithm agrees with the actual electric locomotive wheel load.

3.1 | Axial strain based method

In this method, the axial strain is used to determine the wheel loads.

From the shear strain time history, the location of wheel loads at any given instant in time is determined using the algorithm explained in the Section 2. Knowing the location of the wheel loads at i^{th} time instance, the influence line coordinate for bending moment at a section x distance form the left support of the j^{th} wheel load can be computed as $\mathcal{I}_j^M(x, t_i)$ using the Müller-Breslau's principle. Hence, the bending moment at i^{th} time instance, t_i is

$$M(x, t_i) = \sum_{j=1}^{q} \mathcal{I}_j^M(x, t_i) P_j, \tag{3}$$

where P_j is the magnitude of the j^{th} wheel load, x is the location of the section from the left support, and q is the total number of wheel loads. Assuming that for the material that the bridge is made up of a linear relationship exists between the axial strain and bending moment

$$\epsilon_{axial}(x, t) = K_m M(x, t), \tag{4}$$

where, K_m is a proportionality constant and ϵ_{axial} is the axial strain. It follows from Equations 3 and 4 that if $\{\boldsymbol{\epsilon}_{axial}\}$ is a column vector of axial strains at a given location for different time instances, then

$$\{\boldsymbol{\epsilon}_{axial}\} = [\mathbf{L}^M]\{\mathbf{P}\}, \tag{5}$$

where the vector, $\{\mathbf{P}\}$ represents the unknown wheel loads and the ij^{th} component of $\mathbf{L}^M$ is $K_m \mathcal{I}_j^M(x, t_i)$. It should be noted that the matrix, $\mathbf{L}^M$ is not a square matrix; its dimensions would be the number of data points in the axial strain time history, n, times the number of wheel loads, q. Thus, the wheel loads are determined by pseudo-inversion of the nonsquare matrix $[\mathbf{L}^M]$, which tantamount to finding the wheel loads such that the root mean square error between the measured and the predicted axial strain is minimized.

Here, the entire time history of the axial strain is used to find the wheel loads because the location of the loads that causes the maximum axial strain depends on the magnitude of the load that needs to be computed. It is for the same reason that the position of the wheel loads that causes the maximum axial strain is not known a priori, estimation of wheel speeds based on axial strain time history is susceptible to inaccuracies.

3.2 | Shear strain based method

This method uses the peak shear strain values measured at a location. Unlike in the case of the bending moment, the location of the loads that cause the maximum shear force is independent of the magnitude of the wheel loads.[10] Let $\mathcal{I}_j^V(x, t_i)$ be the influence line coordinate for shear force at a section located at a distance of x from the left support of the j^{th} wheel load at the time of occurrence of the i^{th} peak in the shear strain, t_i. Then, the shear force, V, at an axial location, x from the left support and at time of occurrence of the i^{th} peak in the shear strain time history, t_i is

$$V(x, t_i) = \sum_{j=1}^{q} \mathcal{I}_j^V(x, t_i) P_j. \tag{6}$$

Assuming that for the material that the bridge is made up of a linear relationship exists between the shear strain*, ϵ_{shear} and shear force

*This is half the change in angle between line elements initially oriented along x and y directions, that is the tensorial shear stain component.

$$\epsilon_{shear}(x,\, t) = K_s V(x,\, t), \tag{7}$$

where, K_s is a proportionality constant and ϵ_{shear} is the shear strain. Combining Equations 6 and 7, the peak shear strains represented as a column vector, $\{\epsilon^{max}_{shear}\}$ is related to the column vector of wheel loads, $\{\mathbf{P}\}$ through

$$\{\epsilon^{max}_{shear}\} = [\mathbf{L}^V]\{\mathbf{P}\}, \tag{8}$$

where the ij^{th} component of $\mathbf{L}^V$ is $K_s \mathcal{I}^V_j(x,\, t_i)$. Thus, if there were q wheel loads, there should be q values of peak shear strain and the matrix $[\mathbf{L}^V]$ would be a square matrix of dimensions $q \times q$. Then, the wheel loads are estimated by solving the above 8 system of linear equations.

This algorithm based on shear strain seems to have the following advantages in comparison with that based on axial strain as follows:

(a) **Weakly sensitive to the boundary conditions:** For three extreme boundary conditions—simply supported, fixed-fixed, and propped cantilever, the maximum bending moment at mid-span, maximum shear force at quarter span, and three-quarter span are due to a single point load of magnitude P moving over these three beams having the same span, L is tabulated in Table 1. It can be seen from the table that the percentage variation in the shear force is less than approximately 22%(=7/32 × 100), whereas the variation in the bending moment is 50%. Thus, it is evident that using shear strain would result in a better estimate of the wheel loads even if there is some rotational rigidity due to bearing seizure.

(b) **Estimate of the wheel loads is insensitive to the speed of the train:** Because only the peak strain values are used, the shear strain algorithm becomes insensitive to the speed of the train. It is known that the maximum bending moment and hence, the axial strain need not occur when the train of moving loads is exactly on top of the measurement point (see[10]). Further, the location of the loads for which the maximum bending moment occurs depends on the magnitude of these loads. Hence, one should necessarily use the entire axial strain time series for finding the wheel loads. Also, it can be inferred from modal dynamic analysis that the inertial forces, which depend on the wheel speed influence the axial strains more than shear strain. Experimental measurement of the axial and shear strain by[13] also confirms this observation.

(c) **Accelerating or decelerating forces weakly influence the estimate of the wheel loads:**Braking or acceleration applies an axial force and a moment in the rail, which induces axial and shear strains in the girder, as would be shown in Section 3.2.1. However, the developed axial strain is three times more than that of the shear strain. Thus, algorithms based on axial strain needs a correction for braking or accelerating force whereas those based on shear strain may not require this correction.

(d) **Not influenced by temperature induced strain:** Uniform temperature changes in the girder does not cause distortion and hence, no shear strain. Further, restraint to the free expansion of the continuous rail on top of the girder induces axial strain in the girder. Thus, the axial strain is affected by environmental induced temperature variations but the magnitude of the shear strain changes only minimally.

(e) **Computationally efficient:** The method based on shear strains requires only the inversion of a square sparse matrix of size equal to the number of wheel loads. However, in case of axial strain algorithm, one has to pseudo–inverse a matrix of dimensions number of time points in the time history times the number of wheel loads. Hence, axial strain algorithm is computationally costly.

(f) **Requires less number of sensors:** Because shear strain based algorithm to estimate the wheel load requires only the shear strain at a point, it requires only one strain rosette. Whereas for axial strain based algorithm, the speed of the train needs to be known in addition to axial strain at a point. The speed of the train cannot be estimated

TABLE 1 Theoretical maximum bending moment and shear force for beams with various boundary conditions due to a single moving load of magnitude P

Boundary condition	Max. moment at $L/2$	Max. shear force at $L/4$	Max. shear force at $3L/4$
Simply supported	$PL/4$	$3P/4$	$3P/4$
Fixed-fixed	$PL/8$	$3/4(1+1/8)P$	$3/4(1+1/8)P$
Propped cantilever	$PL/4(1-3/8)$	$3/4(1+7/32)P$	$3/4(1-5/32)P$

correctly using the axial strain time history because, the location of the wheel at which the maximum axial strain occurs at a section depends on the magnitude of the wheel load which is to be found. Hence, shear strain time history is required to determine the speed of the wheels. Thus, in case of wheel load estimation from axial strain time histories, both shear and axial strain needs to be measured. Hence, the number of minimum required sensors is more in case of axial strain algorithm.

However, there are certain shortcomings in the shear strain based algorithms.

(a) **Relationship between shear strain and shear force:** For steel bridges, it is known that the shear strain and stress would be related linearly in the operating stress range. Further, the relationship between shear stress and shear force would be linear. Consequently, it can be established that the shear strain at a location would be linearly related to the shear force at that section. However, for concrete structures, this relationship between shear strain and shear stress need not be linear in the operating stress range. Thus, one has to establish the nonlinear relation between the shear strain and shear force for concrete bridges before this method can be applied.
(b) **Accuracy of measurement of shear strain:** Because the shear strain is determined from three normal strain measurements and its magnitude for real life structures being smaller in comparison with the axial strains, the influence of experimental noise would be more. Consequently, it is expected that the shear strain based inferences would be less robust than axial strain measurements. Although this is true, in general, advances in sensing technology and noise reduction techniques have ensured the robustness of shear strain based inference is only marginally inferior to axial strain based decision provided no other factor influences these strain values. However, it is known that axial strain is influenced by accelerating or decelerating forces or temperature variations or both in the present application.

To summarize, use of shear strains seem to be advantageous for the BWIM application, especially in steel bridges.

3.2.1 | Influence of accelerating or decelerating force

For the speed of the train to decrease or increase, at the wheel rail interface, there would be a traction acting on the top surface of the rail. This acceleration or deceleration causing traction induces a strain which adds to the strain caused due to the wheel loads.

In this section, an estimate of the axial and shear strain in the bridge girder caused due to this traction at the wheel rail interface is made.

When this acceleration or deceleration causing traction occurs over the span of the bridge under consideration, it can be idealized into an axial force, S, acting at the centroid of the cross section of the bridge girder along with a concentrated moment of magnitude, $S(h+a)/2$, where S is the magnitude of the applied traction acting along the axis of the bridge girder, h is the depth of the girder, and a is the depth of the rail. Thus, the axial force, S, induces axial strain and the concentrated moment alters the support reactions and hence, the shear force and the bending moment at a section.[14,15] In addition to this, there is a concentrated moment $Sa/2$ acting on the rail centroid at the point of contact of the wheel and the rail due to the eccentric nature of the traction to the centroid of the rail. This causes vertical deformation of the rail and hence, induces axial and shear strain in the bridge girder.

As a first approximation, the rail could be considered as a beam on elastic foundation, as depicted in Figure 1, with the girder being the foundation that offers the resistance to rail deformation. The resistance offered by the girder depends on its end condition and is never uniform along its axis. In fact, at the supports the girder would have theoretically infinite resistance and the least resistance at mid section. However, as a first approximation, the girder is assumed to offer uniform resistance along its axis. Further, it is assumed that the resistance offered by the girder is proportional

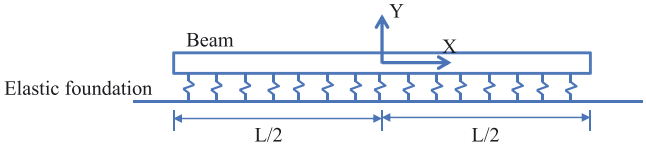

FIGURE 1 Beam on elastic foundation

to the vertical displacement of the rail. Thus, the rail has to be idealized as a beam column resting on an elastic foundation. However, here the buckling effects due to the axial compression in the rail is ignored and the moment ($Sa/2$) alone is assumed to cause vertical displacement of the rail. Using the standard results from the analysis of beam on an elastic foundation subjected to concentrated moment,[16] the support reaction on the rail is computed to be:

$$q_y = \begin{cases} -Sa\beta^2\exp(-\beta(s-b-s_c))\sin(\beta(s-b-s_c)) & \text{if } s \geq b+s_c \\ -Sa\beta^2\exp(\beta(s-b-s_c))\sin(\beta(s-b-s_c)) & \text{if } s \leq b+s_c \end{cases}, \tag{9}$$

where,

$$\beta^2 = \sqrt{\frac{K_s}{4E_{rail}I_{rail}}}, \tag{10}$$

K_s is the constant stiffness offered by the bridge girder per unit length to the deflection of the rail, E_{rail} is the Young's modulus of the rail and I_{rail} is the moment of inertia of the rail cross section about the axis of bending, b is the distance of the applied traction, S from the point of measurement, s denotes the distance of a section on the girder from the left support, and s_c, is the location of the measurement point from the left support.

The support reaction (9) becomes the load per unit length on the bridge span under consideration. For this loading, the expression for the bending moment, M, at mid-span and the shear force, V, at quarter span is given in Appendix .

Now assuming that the material that the steel bridge is made up of obeys isotropic Hooke's law, the axial strain in the mid-span at a location y from the neutral axis is given by,

$$\epsilon_a = \begin{cases} \dfrac{My}{E_{beam}I_{beam}} + \dfrac{S}{E_{beam}A_{beam}}, & \text{if } -L/2 \leq b \leq L/2 \\ \dfrac{My}{E_{beam}I_{beam}}, & \text{otherwise.} \end{cases}, \tag{11}$$

where E_{beam} is the Young's modulus of the beam, I_{beam} is the moment of inertia of the cross section of the beam about the axis of bending, A_{beam} is the area of the cross section of the beam. Similarly, the shear strain in the quarter span at the centroid of the cross section due to shear force V is computed as

$$\epsilon_s = V\frac{(1+\nu)A_s y_s}{EI_{beam}b_s}, \tag{12}$$

where, A_s is the area of the cross section of the beam above the location of the strain gauge, y_s is the centroid of the area of the cross section of the beam above the location of the strain gauge, b_s is the width of the cross section at the location of the strain gauge and ν is the Poisson's ratio of the material that the cross section of the beam is made up of.

To draw meaningful conclusions, both the axial strain and shear strain are normalized with the axial strain produced by the breaking force when on the instrumented span, $S/E_{beam}A_{beam}$ and rearranging the axial strain reduces to,

$$\frac{E_{beam}A_{beam}\epsilon_a}{S} = \begin{cases} f_m\dfrac{ay}{r^2} + 1, & \text{if } -L/2 \leq b \leq L/2 \\ f_m\dfrac{ay}{r^2}, & \text{otherwise,} \end{cases}, \tag{13}$$

where r is the radius of gyration of the cross section of the beam, f_m is given in Equation (A1) and the shear strain evaluates to,

$$\frac{E_{beam}A_{beam}\epsilon_s}{S} = f_s\frac{a(1+\nu)A_s y_s}{2Lr^2b_s}. \tag{14}$$

with f_s given in Equation (A2).

For typical steel I-girders used in medium span railway bridges, looking at the extreme fibre ($y = h/2$) in the section, r^2/y approximately evaluates to,

$$2\frac{r^2}{y} \approx \frac{h}{6}\left(\frac{3+\frac{A_w}{A_f}}{1+\frac{A_w}{A_f}}\right) \tag{15}$$

where, A_w is area of the web and A_f is the area of both the flanges of the I-girder. Practically, A_w/A_f could vary between 0 and 1. Hence, the axial strain geometric factor ay/r^2 would range from $2a/h$ to $3a/h$. Typically, the depth of the rail (a) is between 16 to 17.5 cm and depth of the built up girder varies between 100 to 200 cm. Therefore, h/a could take values between 5 and 12. Therefore, ay/r^2 is taken to vary from 0.15 to 0.6. Recognizing that higher the value of this geometric factor the more would be the value of the axial strain, variation between 0.15 and 0.3 is considered. Figure 2 plots the variation of the axial strain at mid-span for various values of the axial strain geometric factor and material factor βL when h/a is 11. Because, practically h/a could vary between 5 and 12, the value of 11 is chosen for illustration.

Similarly, for typical I shaped steel girders used in medium span railway bridges, the geometric parameter for shear strain,

$$\frac{a(1+\nu)A_s y_s}{2Lr^2 b_s} \approx 0.65[0.15,\ 0.6]\frac{h}{L}\frac{A_f}{2A_w}. \tag{16}$$

Typically, for plate girder bridges, h/L would vary between 1/12 and 1/18, and A_f/A_w practically would lie between 1 and 10. Thus, the geometric factor for shear strain varies between 0.005 and 0.1. Recognizing that lower the value of this geometric factor, lower would be the value of the shear strain, a variation between 0.02 and 0.08 is studied. Figure 3 plots the variation of the shear strain at the quarter span for various values of the shear strain conversion factor and the nondimensional parameter, βL when h/a is 11. Comparing the Figures 2 and 3, it is evident that the magnitude of the shear strain caused due to breaking force is at least three times lesser than the resulting axial strain.

4 | FIELD IMPLEMENTATION

The bridge chosen for the study is Bridge No. 85 (KM 98/400) on Nagari River, at Nagari in Chennai-Mumbai railway corridor. It is a steel plate girder bridge with 12 spans each of length approximately 13.3 m. The bridge is in good condition. Around 20 to 30 trains cross the bridge per day with speeds ranging from 10 to 110 km/h. Initial inspection and investigation gave no visible sign of distress or corrosion. Each of the span consisted of two web stiffened I-girders connected through X-bracing in the cross section at quarter span intervals, and K-bracing in the top (see Figure 4). Individual member dimensions, provided by the Southern Indian Railways and checked in the field, are used for computation of section properties. The cross sectional details of the built up I-section used for the computation of the section properties are as shown in Figure 5. Thus, the beam is not prismatic as an additional 10 mm plate has been added both at the top and bottom of the girder between quarter and three-quarter span.

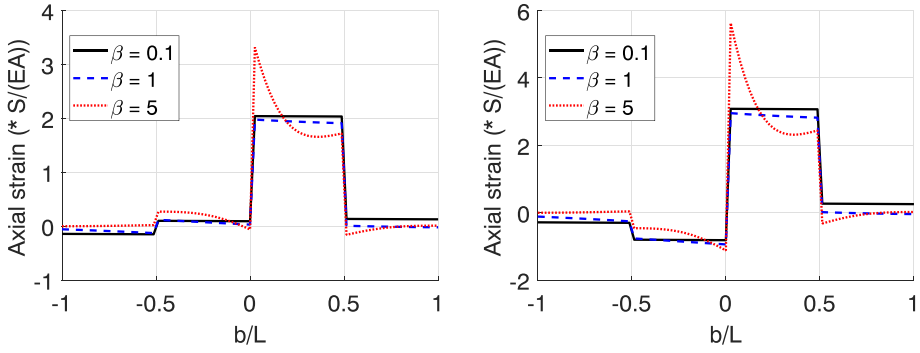

(a) Axial strain geometric factor, $\frac{ay}{r^2} = 0.15$ **(b)** Axial strain geometric factor, $\frac{ay}{r^2} = 0.30$

FIGURE 2 Normalized axial strain at mid-span due to a breaking force at a distance b from the mid-span for various axial strain geometric factor ($\frac{ay}{r^2}$) and material factor (βL)

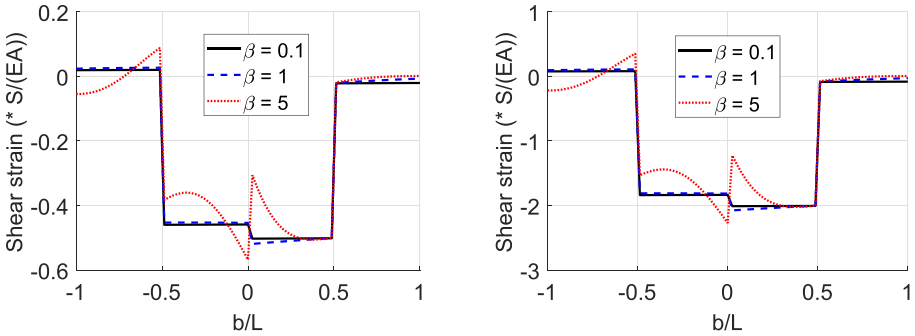

(a) Shear strain conversion factor, $\frac{a(1+\nu)A_s y_s}{2Lr^2 b_s} = 0.02$ **(b)** Shear strain conversion factor, $\frac{a(1+\nu)A_s y_s}{2Lr^2 b_s} = 0.08$

FIGURE 3 Normalized shear strain at quarter span due to a breaking force at a distance b from the mid-span for various shear strain geometric factor ($\frac{a(1+\nu)A_s y_s}{Lr^2 b_s}$) and material factor ($\beta L$)

FIGURE 4 Picture of the instrumented bridge

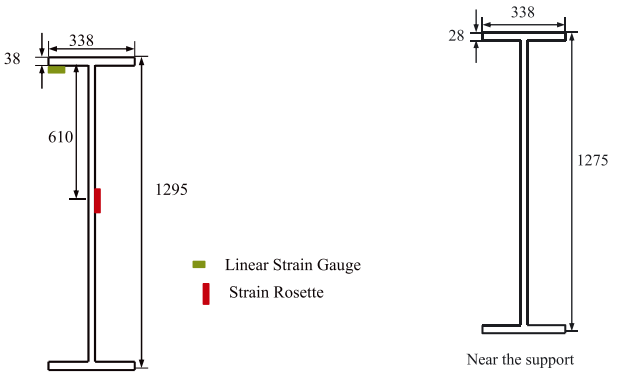

(a) Strain gauge locations **(b)** Girder cross section near the support

FIGURE 5 Strain gauge locations at the mid-span section of the bridge girder and the cross section of the bridge girder near the support

Based on the algorithms to find speed and wheel load, one of the two I-girders in the second span of the bridge is instrumented with 12 wired strain gauges, at various locations—approximately one fourth the span from either end or at the mid-span of the girder. At these locations, a strain rosette is located at the centroid of the cross section to

get the shear strain, and a linear strain gauge is located at the bottom of the top flange to measure the axial strain, as shown in Figure 5. All the strain gauges are connected to the data acquisition system placed on the pier of the bridge.

The data acquisition system starts recording the data on receiving a trigger in the digital input channel from a laser motion detector. The data are recorded at a rate of 200 samples per second for 300 s. The data are stored as date and time stamped binary file. The data are recorded 24×7 whenever a train passed the bridge, for a total of 125 days. During this recorded period, 916 passenger train, 276 Electric Multiple Unit (EMU) train, 69 electric locomotive alone, and 1,171 freight train passed the bridge. EMU is a commuter rail system for semiurban and rural areas in India. In the forthcoming subsections, the computation of speed and wheel loads are explained using two sample train passes—a passenger train and a fully loaded freight train.

The I girder is designed to be simply supported at the ends. If there is sufficient rotational restraint to alter the value of the maximum bending moment that occurs at mid-span, then at a section close to the support there would be a reversal of curvature when a point load moves over the beam. For the bridge under investigation, no reversal of curvature is observed at quarter and three-quarter span when a single electric locomotive passed over the bridge. Hence, the considered girder is taken as a simply supported beam.

The built up steel I-section is assumed to be homogeneous, isotropic, and linear elastic obeying Hooke's law with Young's modulus, $E_{beam} = 200$ GPa.

For symmetrical bending, the axial strain at a distance, $\bar{y}$ from the neutral axis is related to the bending moment, M, through the equation,

$$\epsilon_{axial}(x, t) = \frac{\bar{y}}{E_{beam}I_{beam}} M(x, t) = K_m \times M(x, t), \tag{17}$$

where, $E_{beam}I_{beam}$ is the flexural rigidity of the beam. Theoretically, the value of the proportionality constant, K_m is 2.5×10^{-10} 1/nm for the assumed value of the Young's modulus and the measured section dimensions.

The wheel loads of electric locomotive would nearly be a constant, 102.5 kN (as per the standards provided by the Indian Railways for the locomotive type used—WAG7). Using this locomotive load and the axial strain measured from the field, the proportionality constant, K_m is determined so that it results in the least error in the determined wheel load. The error measure used is,

$$\delta_{\epsilon_{ax}} = \sum_{i=1}^{N} \left(K_m \times M(x, t_i) - \epsilon_{axial}(x, t_i)\right)^2, \tag{18}$$

where $M(x,t_i)$ is the theoretically estimated bending moment at the instrumented location at a distance x from the left support and at time t_i with the wheel loads assumed to be 102.5 kN, $\epsilon_{axial}(x,t_i)$ is the axial strain measured in the field at a distance x from the left support at time, t_i. The value of this proportionality constant, K_m, at a given section located at a distance x from the support and for different velocity ranges is tabulated in Table 2. From the table, it is observed that the value of K_m do not vary significantly with the speed of the train.

The field determined value of K_m has a variation of 2 to 27% from the theoretically estimated value of K_m. The flexural rigidity offered by the rails, K-bracing at the top and X-bracing connecting the two I-girders are not considered in the theoretical estimate. The moment of inertia for the bridge girder alone is $1.2 \times 10^{10} mm^4$. Assuming that there is no

TABLE 2 Mean and standard deviation (SD) of the proportionality factor, K_m, determined from the filed data to convert bending moment to axial strain at various locations and ranges of speed for locomotive alone passes assuming standard load

Velocity interval (km/h)	Quarter-span ($\times 10^{-10} 1/Nm$)		Mid-span ($\times 10^{-10} 1/Nm$)		Three-quarter span ($\times 10^{-10} 1/Nm$)	
	Mean	**SD**	**Mean**	**SD**	**Mean**	**SD**
10–30	2.59	0.05	2.04	0.05	1.85	0.06
30–50	2.54	0.09	2.00	0.05	1.80	0.11
50–70	2.53	0.11	2.03	0.07	1.79	0.04
70–100	2.51	0.01	2.04	0.06	1.81	0.07
10–100	**2.54**	0.06	**2.03**	0.06	**1.81**	0.07
Theoretical	2.50	-	2.50	-	2.50	-

slip between the rail and the girder, the effective moment of inertia of the I - girder with the rail on top is $1.5\times10^{10}mm^4$ (see Figure 6). Of course the rail does not sit directly on the girder, and its contribution to the stiffness depends upon the connection detail between the girder and the rail that could allow some slippage. Thus, a 25% increase in moment of inertia occurs on considering the rail. This suggest that 27% variation due to rails and secondary elements is reasonable. The variation of K_m with the location in the actual structure is because an additional plate has been added at the top and bottom of the I girder from quarter to three-quarter span, making the beam nonprismatic. Hence, rigidity to bending is different at various locations resulting in the value of K_m to change.

The shear strain, ϵ_{shear} at the measured location is related to the shear force, V using the relation,

$$\epsilon_{shear}(x,\ t) = (1+\nu)\frac{A_s y_s}{E_I b_s}V(x,\ t) = K_s \times V(x,\ t), \tag{19}$$

where, A_s is the area of the cross section above the location of the strain gauge, y_s is the centroid of the area of the cross section above the location of the strain gauge, b_s is the width of the cross section at the location of the strain gauge, and ν is the Poisson's ratio of the material that the cross section is made up of. The theoretical value of the constant, K_s is $5.5\times10^{-10}1/N$ on assuming the Poisson's ratio for steel to be 0.3.

Here again, the field data from the electric locomotive passes with known wheel loads is used to find the constant K_s for a given section at a distance x from the left support. The value of the proportionality constant K_s is estimated by minimising the error defined as,

$$\delta_{\epsilon_{sh}} = \sum_{i=1}^{N}(K_s\times V(x,t_i) - \epsilon_{shear}(x,t_i))^2, \tag{20}$$

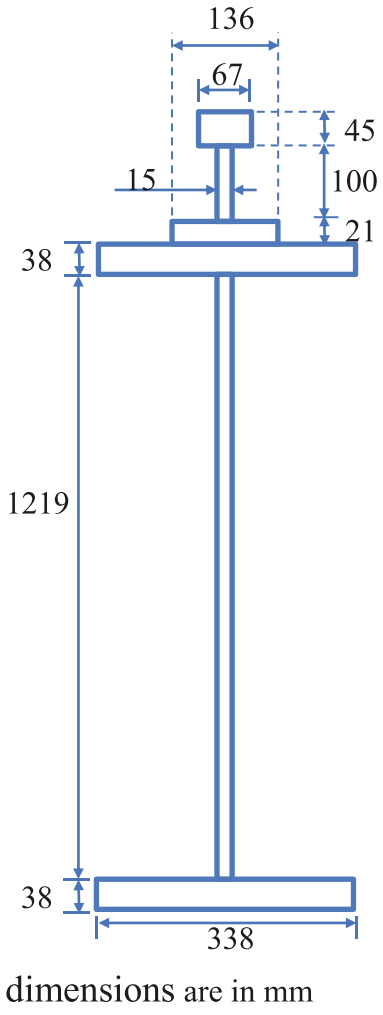

FIGURE 6 Cross sectional details of the bridge girder along with the rail on top of it

where $V(x, t_i)$ is the theoretically estimated shear force at the instrumented location at a distance x from the left support and at time t_i with the wheel loads assumed to be 102 kN, $\epsilon_{shear}(x,t_i)$ is the shear strain measured in the field at a distance x from the left support at time, t_i. The so determined value of the constant, K_s at various instrumented locations is tabulated in Table 3. The observed larger variation in the value of K_s at mid-span is because of the shear strain is close to 0 at this location. Even otherwise, the maximum magnitude of the shear strain is less than half the maximum magnitude of the axial strain that results in larger variation in the determined K_s values (standard deviation: 0.13 at quarter span, 0.25 at mid-span, and 0.14 at three-quarter span). Assuming the noise levels to be the same because the signal strength is halved, the standard deviation in K_s is twice that of in K_m. Further, statistical test show that the observed difference in the mean value of K_s is not significant.

The field determined value of K_s is around 25 to 7% lower than the theoretical estimate. Because the flexural rigidity of the beam, EI_{beam}, differs, for reasons discussed above, the value of this constant K_s also varies by around similar percent. Though the data pertaining to the variation of the constant, K_s with the speed of the train is not presented, no statistically significant variation is observed.

Having found the required parameters in the model, the results of the algorithms are presented and issues with the algorithms discussed.

4.1 | Estimation of wheel speed—Illustrative example

It is expected that a peak occurs when each wheel load is above the point of measurement. But in the data recorded from the field for shear strain, only one peak is observed each for the front and rear bogie wheel sets. This has been observed in earlier studies also.[8] Thus, in the estimation of the configuration of train and load position equation, the wheel loads in a bogie are added together and the resultant is considered so that peaks are obtained as observed in the field data. For locomotives, the front and rear bogie consist of three wheel loads whereas for wagons, the front and rear bogie consist of two wheel loads each. From influence line diagram for shear force at section X on the girder, given in Figure 7, it is observed that the peak in the shear strain occurs when the first load of the bogie is at a distance, c from the measurement point. Here c is half the distance of the spacing between the sleepers.

Consider a passenger train that crossed the bridge on August 4, 2014, 8:30 hours. The shear strain data at three-fourth span is plotted in Figure 8 with the peaks identified. For a passenger locomotive, each bogie consist of three axles of 20.5 tonnes each. Thus, the three wheels of a locomotive bogie gives 30.75 tonnes. In contrast, each bogie of the wagon consists of two axles and the maximum allowable load in the axle of passenger wagons is 16.25 tonnes. Thus, the total maximum wheel load for a bogie in passenger wagon is 16.25 tonnes. Hence, the axial and shear strains induced due to the wagons are less than that due to the locomotive. With this background, from the magnitude of the peaks, the first two peaks are identified as that corresponding to the front and rear bogies of the locomotive and the following 34 peaks as being that of the 17 wagons. Having determined the configuration of the train, the axle spacings become know. Using this axle spacing and the time of occurrence of the peaks in the shear strain time history, the polynomial (1), for this train, is determined using the methodology elaborated in Section 2 as

$$s = -0.0003t^4 + 0.0084t^3 - 0.1875t^2 + 25.87t, \quad \text{m}, \tag{21}$$

TABLE 3 Mean and standard deviation (SD) of the proportionality factor, K_s, determined from the filed data to convert shear force to shear strain at various locations and ranges of speed for locomotive alone passes assuming standard load

Velocity interval (km/h)	Quarter-span ($\times 10^{-10} 1/N$)		Mid-span ($\times 10^{-10} 1/N$)		Three-quarter span ($\times 10^{-10} 1/N$)	
	Mean	**SD**	**Mean**	**SD**	**Mean**	**SD**
10–30	3.73	0.15	5.07	0.27	5.03	0.16
30–50	3.94	0.14	4.39	0.54	5.00	0.21
50–70	4.10	0.16	4.09	0.05	5.18	0.11
70–100	4.44	0.08	3.84	0.14	5.08	0.08
10–100	**4.05**	0.13	**4.35**	0.25	**5.07**	0.14
Theoretical	5.50	-	5.50	-	5.50	-

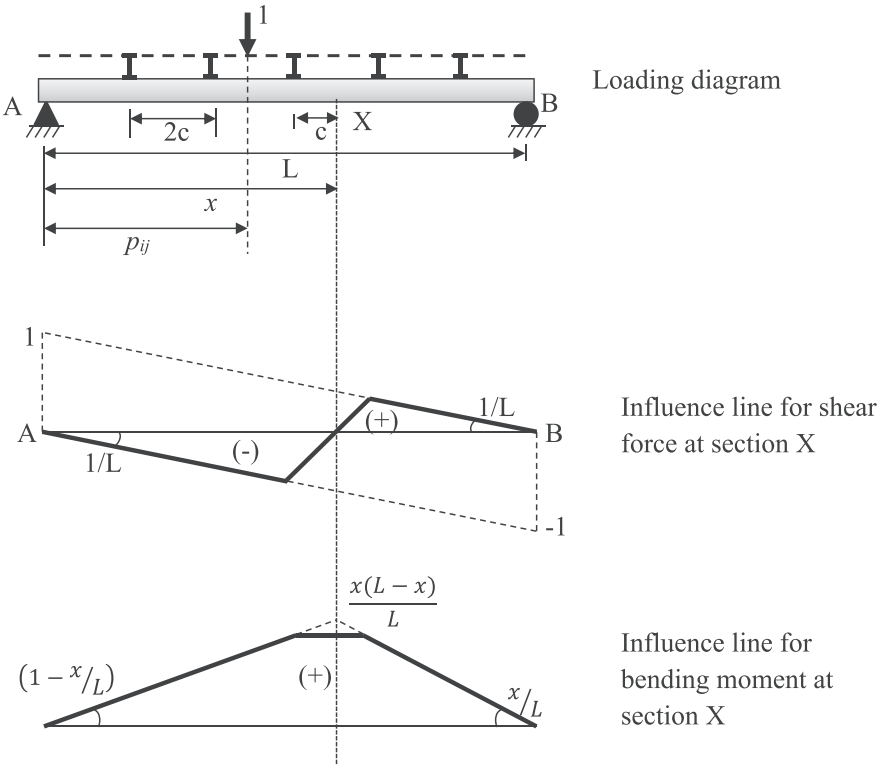

FIGURE 7 Influence line diagram for shear force and bending moment at a section

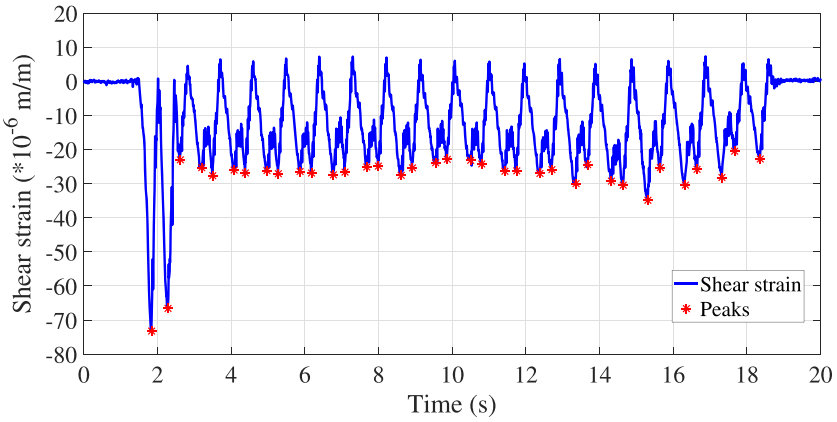

FIGURE 8 Variation of the shear strain at three-quarter span with time of a passenger train passing the bridge on August 4, 2014 at 8:30

where the unit of time, t, is seconds. The adjusted R^2 value for this fit is 0.998. The plot between the axle spacings and the time of occupance of the peaks in the shear strain time history and the best fit that describes it is given in Figure 9. Figure 10 plots the variation of the speed of this passenger train with time, which shows that the speed of the train decreases over time, but at a nonuniform rate.

As another example to illustrate the estimation of speed, consider a freight train that traversed the bridge on March 23, 2014 at 10:50. From the shear strain at three-quarter span time history shown in Figure 11 it can be inferred that the freight train has two locomotives and 52 wagons. Using this shear strain data at three-fourth the span, the best-fit equation that defines the load position is obtained as shown in Figure 12. The best-fit equation for load position is given by,

$$s = -0.000001t^4 + 0.0004t^3 - 0.050t^2 + 7.656t, \quad \text{m} \tag{22}$$

where the unit of t, is seconds. The adjusted R^2 value of fitting this equation is 0.9957. Figure 13 plots the variation of the speed of this freight train with time. It can be seen from Figure 13 that the train decelerated initially and then it began to accelerate. It should be noted that the value of time is of the same order as that of the distance s. Hence, the higher order

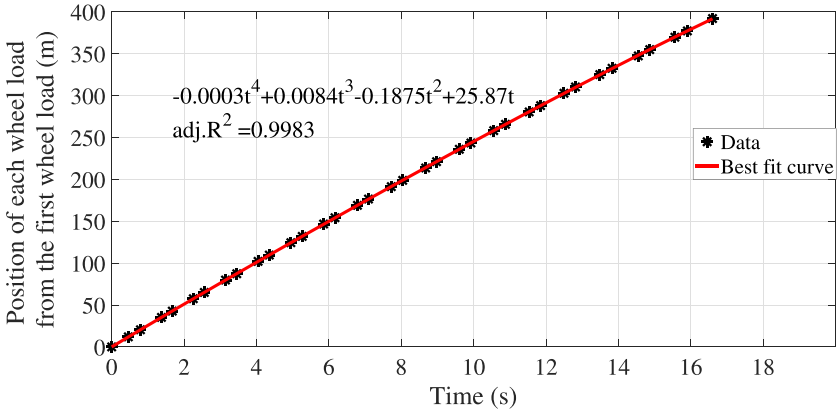

FIGURE 9 Axle spacing with respect to the time of occupance of peaks in the shear strain time history of the passenger train passing the bridge on August 4, 2014 at 8:30

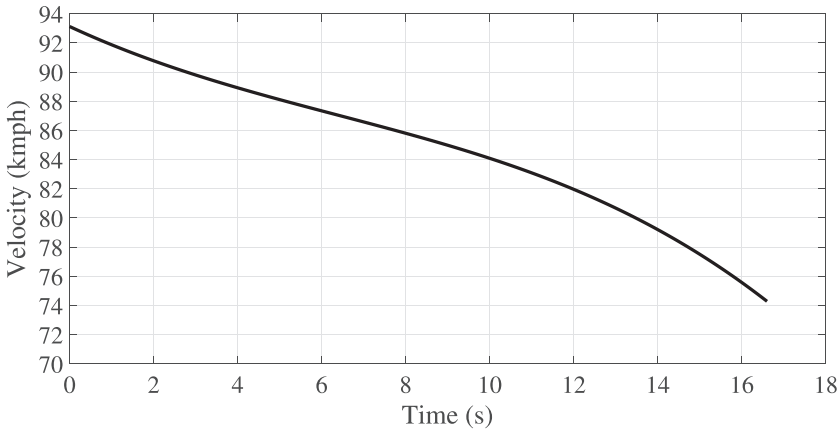

FIGURE 10 Variation of speed with time of a passenger train passing the bridge on August 4, 2014 at 8:30

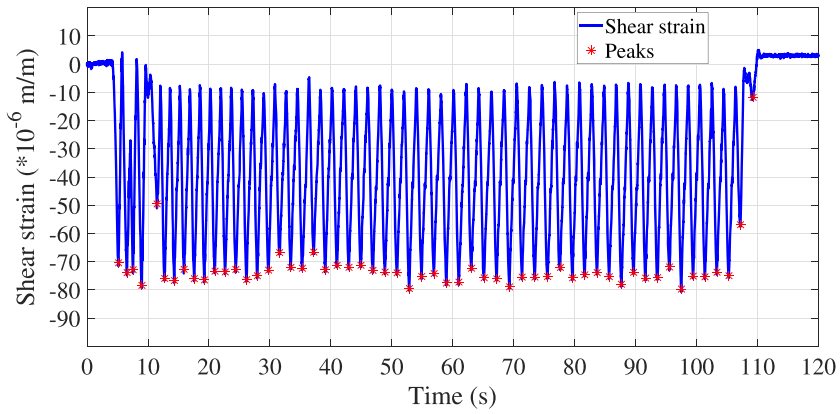

FIGURE 11 Variation of the shear strain at three-quarter span with time of a freight train passing the bridge on March 23, 2014 at 10:50

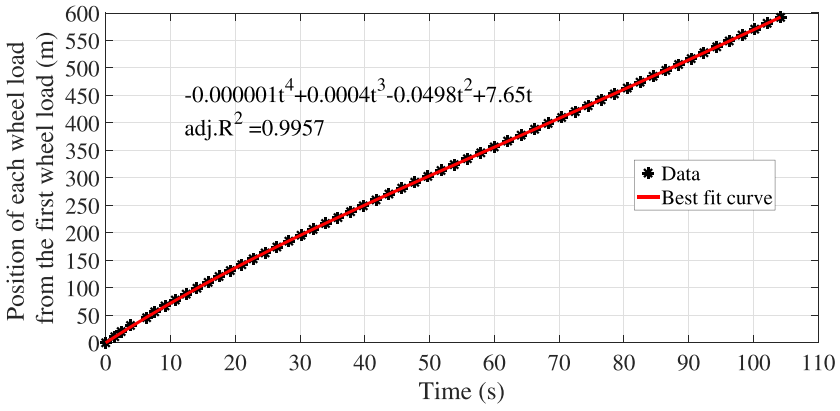

FIGURE 12 Axle spacing with respect to the time of occupance of peaks in the shear strain time history of the freight train on March 23, 2014 at 10:50

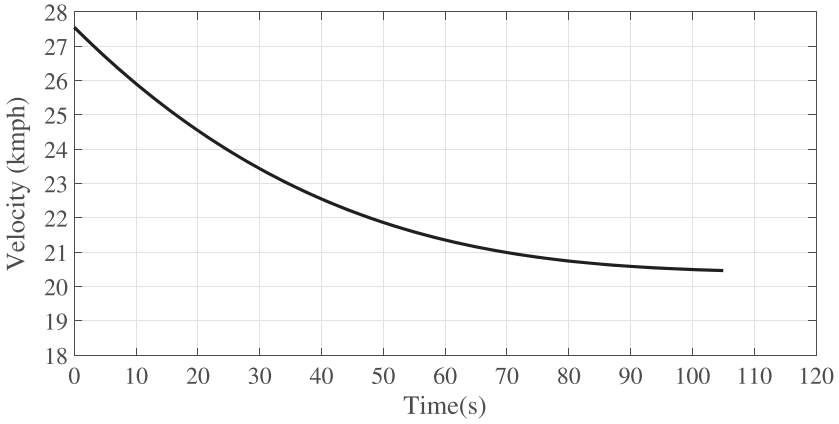

FIGURE 13 Variation of speed of the freight train on March 23, 2014 at 10:50

coefficients of time has to be smaller. Further, 4^{th} power term is included only for trains for which the adjusted R^2 value decreased by inclusion of this term. Hence, the higher order terms cannot be neglected.

It is observed that the valleys in the shear strain time history of the passenger train has values greater than 0 (see Figure 8) but that of the freight train is always less than 0 (see Figure 11). This is because the axle spacing between the front and rear bogie of the passenger train is 11.8 m, which makes it possible to have wheel loads only in sections before the point of measurement making the shear force positive. But for freight trains, the axle spacing between the front and the rear bogie is only 4.5 m. This 4.5 m spacing does not allow for the cases wherein the wheel loads are only on the sections before the point of measurement. Hence, the valleys in the shear strain time history of the freight train is always less than 0.

Thus, the above examples demonstrate that neither the speed nor the acceleration would be constant for trains. In Section 5, the error resulting from the assumption of the uniform speed of the train is illustrated.

4.2 | Estimation of wheel load—Illustrative example

One of the inputs to estimate the wheel loads from measured axial strain is the influence line for the bending moment at the measurement location. If p_{ij} is the position of j^{th} wheel load at i^{th} time instance, and $\mathcal{I}_j^M(x,\, t_i)$ is the bending moment influence line coordinate corresponding to the j^{th} wheel load at i^{th} instance, then

$$\mathcal{I}_j^M(x,\, t_i) = \begin{cases} \left(1 - \dfrac{x}{L}\right) p_{ij}, & \text{if } 0 \le p_{ij} \le x - c \\ \dfrac{1}{2}\Big(p_{ij} + (x - c)\Big), & \text{if } x - c \le p_{ij} \le x + c \\ \left(1 - \dfrac{p_{ij}}{L}\right) x, & \text{if } x + c \le p_{ij} \ \le L \\ 0, & \text{otherwise} \end{cases}, \tag{23}$$

where x is the axial location of the measurement point from the left support, L the span of the simply supported beam, and c is half the distance between the sleepers. Here $c = 0.35$ m. For the axial strain measured at mid-span, Equation (23) and the proportionality factor listed in Table 2 is used in Equation (5) to obtain the wheel loads as detailed in Section 3.1. For the electric locomotives used by the Indian Railways (WAG7 or WAP7 corresponding to freight or long distance passenger trains respectively), there are three axles each in the front and rear and for the wagons there are two axles each in the front and rear.

The individual axle wheel loads determined from the axial strain algorithm are negative in some cases. However, if the loads are clustered such that the three or two axles that comprise the front or rear of the bogie are added, then the clustered loads are all positive. It was also noted that from the wheel loads estimated for all the train passes, the negative loads arise only for some wheels in a few train passes. The negative load indicates the loss of contact between the bridge and the vehicle wheel. The reason for these negative loads to arise needs detailed study.

If $\mathcal{I}_j^V(x, t_i)$ is the shear force influence line co-ordinate corresponding to the j^{th} wheel load at i^{th} instance, then

$$\mathcal{I}_j^V(x, t_i) = \begin{cases} -\dfrac{p_{ij}}{L} & \text{if } 0 \le p_{ij} \le x - c \\ \left(\dfrac{-1}{L} + \dfrac{1}{2c}\right) p_{ij} - \left(\dfrac{x-c}{2c}\right) & \text{if } x - c \le p_{ij} \le x + c \\ 1 - \dfrac{p_{ij}}{L} & \text{if } x + c \le p_{ij} \le L \\ 0 & \text{otherwise.} \end{cases} \tag{24}$$

Further, as already discussed, because peaks in the shear strain time history corresponding to individual axles are not obtained, the axle loads in a bogie are summed and only the total bogie load is found from the shear strain algorithm. Because the wagons are so designed that each of the axles comprising the front or rear of the bogie carries equal load, the estimated resultant load is distributed uniformly to the individual wheels.

The root mean square error between the wheel loads determined by axial strain and shear strain method for this passenger train is 0.58 tonnes. The bogie loads estimated using both the methods are tabulated in Table B1 in the Appendix.

Figure 14 compares the measured axial strain time history at mid-span with that computed using the wheel loads determined by both the axial strain and shear strain method for the passenger train being studied. Figure 15 compares the measured shear strain time history with that computed using the wheel loads by the two methods being studied here for the same passenger train. It can be seen from Figures 14 and 15 that the loads determined by both the methods fit as well as predict the other strain time histories equally well.

The resultant wheel loads for each bogie are determined for a freight train that traversed the bridge on 23rd March 2014 at 10:50 a.m. by both the axial and shear strain based methods. The root mean square error between the wheel loads determined by both these methods is 1.29 tonnes. Whereas Figure 16 compares the measured axial strain with that determined using loads estimated by axial strain and shear strain algorithms, Figure 17 does the same for the shear strain. As with the passenger train, it can be seen from Figure 17 that the fits are good in the case of shear strain. But the computed axial strains do not catch the peaks and valleys of the field strain (see Figure 16). However, the peaks and valleys in axial strain history are well captured when the loads determined from axial strain algorithm are considered without combining for bogie, as shown in Figure 18. But these loads determined from axial strain algorithm without clustering does not predict the shear strain well as shown in Figure 19. The shear strain computed using the loads determined from axial strain algorithm has higher peaks and valleys because some wheel loads have negative value and consequently another wheel load in the same bogie has a high value.

Thus, the question is whether the wheel loads determined from the axial strain algorithm needs to be added with respect to each bogie or not. Because, from the shear strain one obtains only resultant bogie loads, and negative wheel

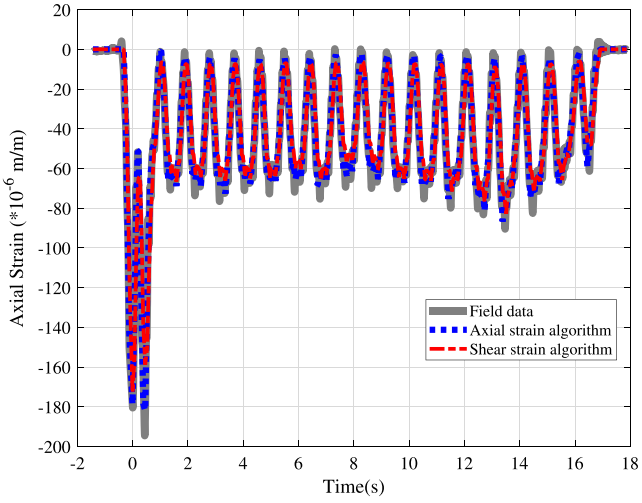

FIGURE 14 Comparison of measured axial strain at mid-span with that computed using the wheel loads determined by axial and shear strain method for the passenger train on August 4, 2014 at 8:30 a.m.

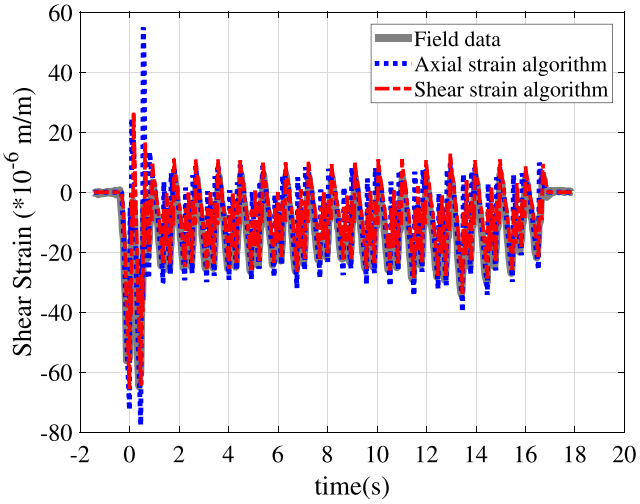

FIGURE 15 Comparison of measured shear strain at three-quarter span with that computed using the wheel loads determined by axial and shear strain method for the passenger train on August 4, 2014 at 8:30 a.m.

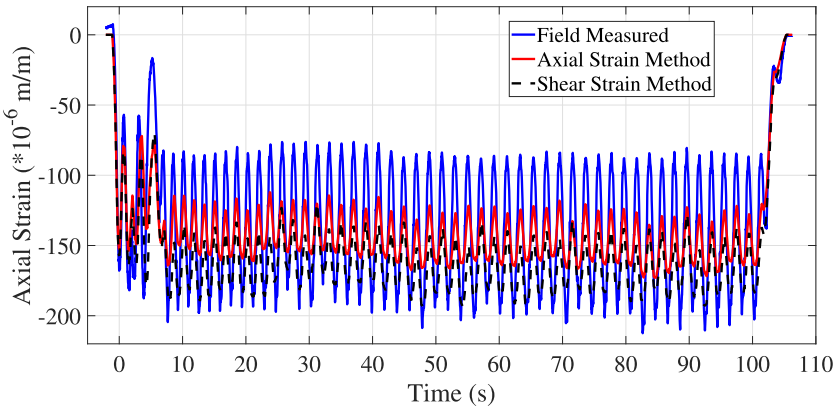

FIGURE 16 Comparison of measured axial strain at mid-span with that computed using the wheel loads determined by axial and shear strain method for the freight train on March 23, 2014 at 10:50 a.m.

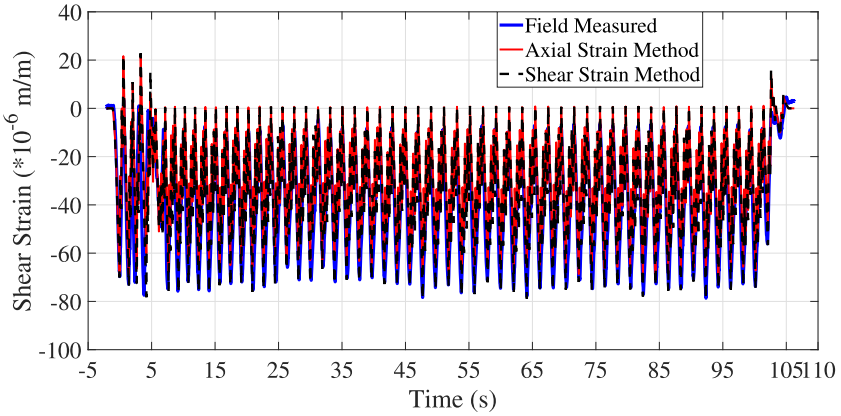

FIGURE 17 Comparison of measured shear strain at three-quarter span with that computed using the wheel loads determined by axial and shear strain method for the freight train on March 23, 2014 at 10:50 a.m.

loads seems impractical, all comparisons with both the algorithms is based on resultant wheel loads determined from axial strain algorithm.

Table 4 tabulates the root mean square error (RMSE) values of the strain time histories at various locations for the two trains being studied. Here, it is pertinent to point out that the maximum value of the shear strain (70 microstrains) is less than half the value of the maximum axial strain (185 microstrains). The expected accuracy in the inferred strain is ±5 micro strains. Thus, it can be inferred from the table that the performance of both the algorithms is equally good for

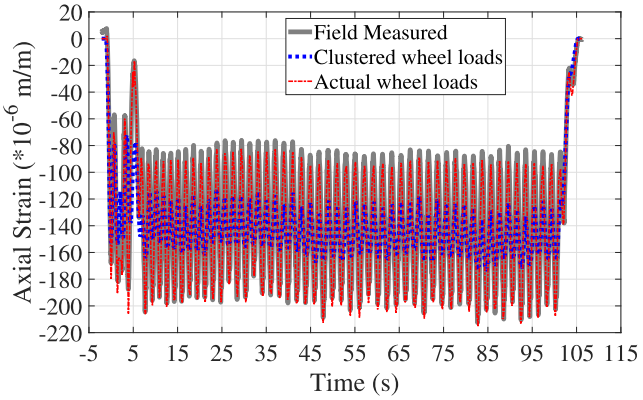

FIGURE 18 Comparison of measured axial strain at mid-span with that computed using the wheel loads determined by axial strain method with and without clustering the bogie loads for the freight train on March 23, 2014 at 10:50 a.m.

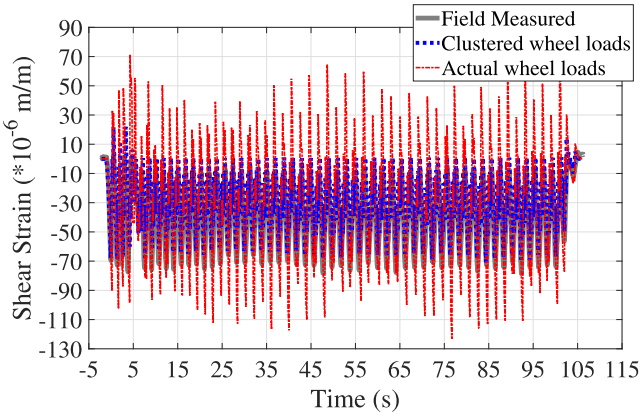

FIGURE 19 Comparison of measured shear strain at three-fourth span with that computed using the wheel loads determined by axial strain method with and without clustering the bogie loads for the freight train on March 23, 2014 at 10:50 a.m.

TABLE 4 Root mean square error between the field measured strain and that computed using the estimated wheel loads using both the methods, for the passenger and freight trains considered (all the values are in microstrain)

	Passenger train		Freight train	
Particulars	**Axial strain algorithm**	**Shear strain algorithm**	**Axial strain algorithm**	**Shear strain algorithm**
Axial strain at $L/4$	8.54	10.35	23.75	30.23
Axial strain at $L/2$	8.55	10.47	27.75	35.23
Axial strain at $3L/4$	8.05	9.22	21.70	26.73
Shear strain at $L/4$	6.66	5.91	14.48	17.27
Shear strain at $L/2$	6.90	6.48	13.47	13.67
Shear strain at $3L/4$	6.90	6.98	15.66	13.81

passenger trains. For freight trains the shear strains are predicted better than that of axial strains. This is because of using clustered bogie loads, as documented above. Moreover, the RMSE in case of shear strain for freight train is nearly twice more than that of passenger train. This may be because of acceleration or deceleration traction in case of fully loaded freight train being order of magnitude more than that of passenger train causes significant shear and axial strains. The dynamic effects and different sensitivity of the parameters K_m and K_s also could manifest in the RMSE error of the freight trains being more than that of the passenger train.

5 | VALIDATION

5.1 | Validation of speed estimation algorithms

The strain time histories computed using the above estimated speeds agree with the field measurement without any phase difference. To illustrate, if the estimated speed is not correct, the computed strain would have a phase difference with the measured strain as seen in Figure 20. Hence, it can be concluded that the speed computed using the developed algorithm is good.

5.2 | Validation of wheel load estimation algorithms

Figure 21 plots the histogram of locomotive wheel load estimated using both algorithms for the case when electric locomotive alone passed over the instrumented bridge span. The figure also plots the locomotive wheel load prescribed

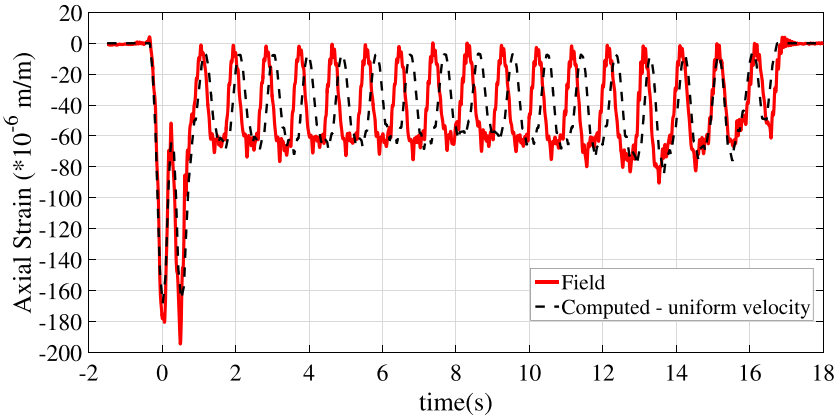

FIGURE 20 Comparison of measured axial strain at mid-span with that computed using the wheel loads determined by shear strain method assuming uniform speed for the passenger train on August 4, 2014 at 8:30 a.m.

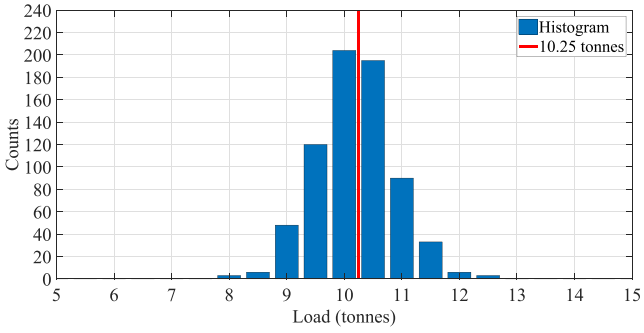

(a) Axial strain algorithm

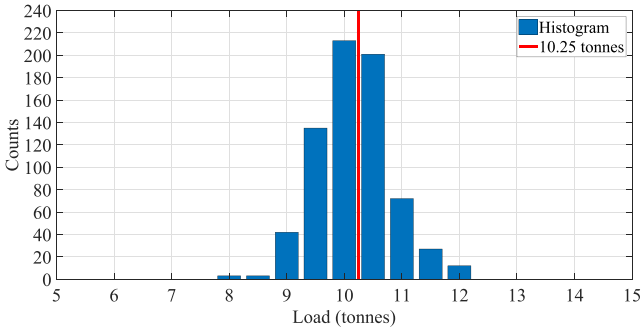

(b) Shear strain algorithm

FIGURE 21 Estimate of locomotive wheel load by the two algorithms when electric locomotive alone passed the bridge

by the standards of Indian Railways. The mean, standard deviation and log-likelihood estimate of the computed wheel load for the electric locomotives for various types of trains are tabulated in Table 5. Here the difference in the electric locomotive for passenger and freight is only in the axle spacings. Because the electrical locomotive weights do not depend on the passenger or freight carried, the weights estimated from the field should agree with the standard weight specified by the Indian Railways. During the observed period, the number of electric locomotive alone passes is 69, passenger train alone passes is 916 and freight train passes is 1,171 that partly explains the difference in the log likelihood estimates across the type of train in Table 5. The log likelihood estimate indicates that both the algorithms are performing equally well for the case of locomotive alone and passenger trains; whereas the shear strain algorithm performing better in case of a freight train. Freight trains that are longer accelerate or decelerate; hence, the axial strain is corrupted by the traction applied on the rails as documented in Section 3.2.1. This is a possible explanation for the shear strain algorithm performing better in the estimate of the electric locomotive loads in case of freight trains.

Further, if the estimated wheel load using strains at a particular location is correct, it should be able to predict the strain time histories at other measured locations. For the shear strain algorithm, the shear strain measured at three-quarter span is used to find the wheel loads. On the other hand for axial strain algorithm, the axial strain measured at mid-span and the shear strain measured at three-quarter span is used. Using the determined wheel loads, one can predict and compare with the measured time histories of the shear and axial strain measured at the quarter span, axial strain measured at three-quarter span, and shear strain measured at mid-span. The root mean square error of the comparison of the predicted and measured strain time history at various locations is tabulated in Table 6 for electric locomotive alone passes. It can be inferred from Table 6 that the estimated loads are robust as it correctly predicts the strain time history at other locations. The mean error in axial strain is less than 10\% of the measured maximum axial strain and the error in the shear strain is less than 15% of the measured maximum shear strain. It is pertinent to observe that the measurement accuracy ($\pm$5 microstrains) is 2.7% in case of axial strain and 7.1% in case of shear strains.

6 | DISCUSSIONS

The resolution of the wheel load in both these methods is different even if the axial and shear strain is measured at locations where they are maximum. For example, in the instrumented bridge, the axial strains is nearly two times

TABLE 5 Mean, Standard deviation and likelihood ratio of the estimated locomotive wheel load for electric locomotive alone for various types of train

	Shear strain algorithm			Axial strain algorithm		
Type of train	Mean (tonnes)	Std. deviation (tonnes)	Log likelihood	Mean (tonnes)	Std. deviation (tonnes)	Log likelihood
Locomotive alone	10.16	0.64	−695.3	10.2	0.66	−713.0
Passenger train	9.29	0.75	−6493.9	10.38	0.76	−6588.6
Freight train	10.04	0.64	−10401.3	9.80	1.06	−15154.6

TABLE 6 Mean and Standard deviation of the RMSE values for strain measured at various locations in the case of electric locomotive alone passes (All the values are in microstrain)

	Shear strain algorithm		Axial strain algorithm	
Particulars	Mean	Std. deviation	Mean	Std. deviation
Axial strain at $L/4$	11.85	3.68	11.41	3.45
Axial strain at $L/2$	13.51	3.96	13.80	5.28
Axial strain at $3L/4$	11.09	4.13	11.14	4.87
Shear strain at $L/4$	11.18	4.64	11.18	4.46
Shear strain at $L/2$	9.84	3.17	9.93	3.08
Shear strain at $3L/4$	12.15	2.83	12.33	2.87

the shear strain. Thus, whereas the axial strain algorithm can resolve one sixth of a tonne, the shear strain algorithm resolves only three eights of a tonne.

Both the algorithms assume that the wheel locations are known a priori. Although this may not be possible in case of roadways, it is achievable in case of railways as the possibilities are few. For example, there are only 15 different electrical locomotives used in India of which in a particular segment only four (one for freight, one for long distance passenger, and two for local trains) would be used. Similarly, there are only one type of passenger wagon and four types of freight wagons. Hence, as outlined and demonstrated in this study, the train configuration is determined based on the recorded shear strain. If the used wheel spacing is incorrect then discrepancy in the time series agreement between the predicted and the field would indicate the same. Of course, the wheel spacing could also be taken as a variable to be found; but this was not done in this study as it was not necessary.

Because the shear strain algorithm utilizes only the peak value of the shear strain, correct determination of the peak values even when there are experimental noises is essential. However, with the current de-noising algorithms this did not prove to be a bottle neck for the collected data. Precautions were taken in the field also to minimize the influence of environmental noise on the signal. Instead of using just the peak values of the shear strain, the entire time history of the shear strain can also be used to estimate the wheel loads, like in axial strain based method. If the full time history of the shear strain is used to estimate the wheel loads, such an algorithm would be computationally costly apart from it depending on the accuracy of the determined speed of the train. For the data considered, both the approaches based on peak shear strain and entire time history of shear strain—gave similar estimates of the bogie loads (for brevity proof for the same is not presented here). Hence, the algorithm based on peak shear strains alone is studied in detail.

The wheel loads determined from the axial strain algorithm are negative in some cases. Some investigations done to understand if these negative loads are due to experimental artifact is documented next. When the wheel loads estimated for all the train passes are considered, the negative loads constitute the tail portion of the distribution as seen from Figure 22. The mean and standard deviation of the individual wheel loads are given in Table 7. Also, when these individual wheel loads are clustered to bogie loads, there are no negative loads, as depicted from the mean and standard values in Table 7. Hence, it is possible that negative wheel loads could be an experimental artifact or a consequence of dynamic response of the bridge.

Only static analysis is done in this study. This is because the strain time histories computed using dynamic analysis with moving force model[17] yielded the same results as the static analysis for the bridge under study, when the speed of the moving loads ranged from 10 to 120 km/h; the measured speed range in the field. As an illustration, a comparison of

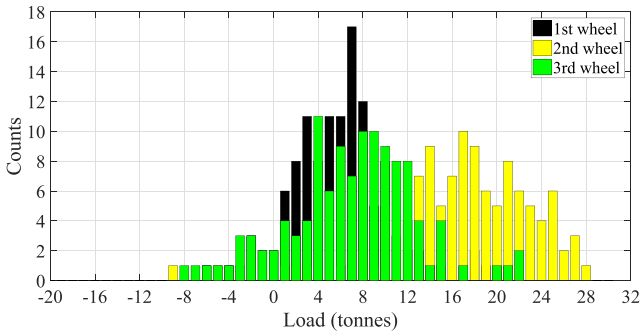

(a) Front bogie wheel loads

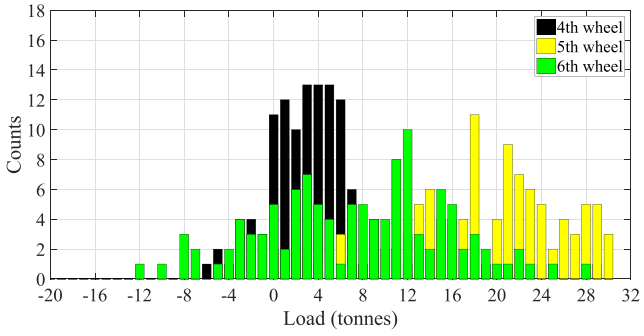

(b) Rear bogie wheel loads

FIGURE 22 Histogram of the individual wheel loads estimated using axial strain method for electric locomotive alone passes

TABLE 7 Mean and standard deviation of the individual wheel loads and bogie loads estimated using axial strain method in the case of electric locomotive alone passes

Wheel load	Mean	Standard deviation	Bogie	Mean	Standard deviation
First wheel	6.15	4.7	First bogie	30.29	2.0
Second wheel	16.72	6.6			
Third wheel	7.00	5.8			
Fourth wheel	3.84	5.4	Second bogie	30.84	2.1
Fifth wheel	18.1	8.0			
Sixth wheel	7.51	8.2			

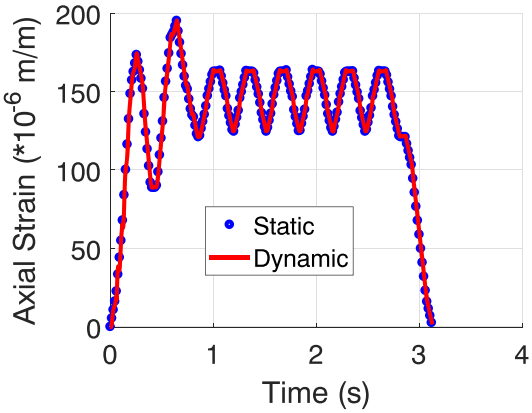

FIGURE 23 Comparison of the computed axial strain at mid-span for dynamic and static analysis

static and dynamic analysis computed axial strain time histories for a train with one electric locomotive and seven wagons moving at 12 km/h is plotted in Figure 23. Standard electric locomotive wheel load of 10.25 tonnes and the wagon load of 8.5 tonnes are assumed for this illustration. Here, a damping ratio of 0.1 is assumed and the cross sectional properties of the investigated girder is used, namely, the cross section flexural rigidity, $E_{beam}I_{beam} = 3\times10^9$ Nm^2 and mass of the cross section, $m = 306$ kg. The root mean square error in the axial strain computed using the dynamic and static analysis is five microstrain, indicating the sufficiency of static analysis for the instrumented bridge under observed speed ranges. It should also be noted that the moving force model would produce the highest deviation of the axial strain from their static values.

7 | CONCLUSIONS

Mechanics based algorithms are developed to estimate the speed and wheel loads of the trains passing over a bridge using the strain data at specific locations. The speed estimation algorithm uses shear strain at quarter span and gives due consideration to the speed variation of the train. For wheel load estimation, two algorithms are studied. The shear strain algorithm utilizes only the peak value of the shear strain measured at an axial location close to the support. On the other hand, the axial strain algorithm utilizes both the axial strain to find the wheel loads and the shear strain to find the wheel speed. The algorithm based on the shear strain seems to have several advantages, namely, (a) less sensitive to changes in boundary condition, (b) estimate of the wheel loads is insensitive to the speed of the train, (c) influence of the accelerating or decelerating forces is the least, (c) least affected due to temperature changes, (d) computationally efficient, and (e) requires less number of sensors. However, it requires accurate determination of the peak shear strain whose magnitude would typically be less than the axial strain in real life bridges. Also, the relationship between the shear strain and shear force must be robust. Thus, beam weigh-in-motion systems utilizing shear strains measured in the girder seem to be robust, especially for steel girders.

ACKNOWLEDGEMENTS

Authors thank the National Program on Micro and Smart Systems (NPMASS) for funding this work through project PARC 3.18. The authors also thank southern railways for allowing and extending all help to monitor the railway bridge.

ORCID

Umakanthan Saravanan http://orcid.org/0000-0001-8565-0632

REFERENCES

1. Sivakumar B, Ibrahim F. Enhancement of bridge live loads using weigh-in-motion data. *Bridg Struct*. 2007;3(3-4):193-204.
2. Bakht B, Mufti A. *Bridges: Analysis, Design, Structural Health Monitoring, and Rehabilitation*. 2nd ed.: Switzerland: Springer; 2015. 425 pp.
3. Moses F. Weigh-in-motion system using instrumental bridges. *Transp Eng*. 1979;105(TE3):233-249.
4. O'Connor C, Chan THT. Dynamic wheel loads from bridge strains. *J Struct Eng*. 1989a;114(8):1703-1723.
5. O'Connor C, Chan THT. Wheel loads from bridge strain: laboratory studies. *J Struct Eng*. 1989b;114(8):1724-1740.
6. Peters RJ. AXWAY - a system to obtain vehicle axle weights. In: Proceedings of 12th ARRB Conference, Vol. 12; 1984; Hobart, Australia:10-18.
7. Grave S. *Modelling of site-specific traffic loading on short to medium span bridges*; Department of Civil Engineering, Trinity College Dublin; 2001.
8. Karoumi R, Wiberg J, Liljencrantz A. Monitoring traffic loads and dynamic effects using an instrumented railway bridge. *Eng Struct*. 2005;27(12):1813-1819.
9. Marques F, Mountinho C, Hu W-H, Cunha A, Caetano E. Weigh-in-motion implementation in an old metallic railway bridge. *Eng Struct*. 2016;13:15-29.
10. Hibbeler RC. *Structural Analysis*. 8th ed.: New York: Pearson Prentice Hall; 2012.
11. Liljencrantz A, Karoumi R, Olofsson P. Implementing bridge weigh-in-motion for railway traffic. *Comput Struct*. 2007;85(1-2):80-88.
12. Znidaric A, Kalin J, Kreslin M, Favai P, Kolaskowski P. Railway bridge weigh-in-motion system. *Transp Res Procedia*. 2016;14:4010-4019.
13. Fafard M, Laflamme M, Savard M, Bennur M. Dynamic analysis of existing continuous bridge. *J Bridg Eng*. 1998;3(1):28-37.
14. Morsch E. The effect of braking forces on solid bridges. *IABSE Congress Report*. 1936;2:819-845.
15. Toth J, Ruge P. Spectral assessment of mesh adaptations for the analysis of the dynamical longitudinal behavior of railway bridges. *Arch Appl Mech*. 2001;71(6–7):453-462.
16. Saravanan U. Advanced Solid Mechanics. http://nptel.ac.in/courses/105106049/; 2013.
17. Snaidy P. Vibration of a beam due to a random stream of moving forces with random velocity. *J Sound Vib*. 1984;97(1):23-33.

How to cite this article: Deepthi TM, Saravanan U, Meher Prasad A. Algorithms to determine wheel loads and speed of trains using strains measured on bridge girders. *Struct Control Health Monit*. 2019;26:e2282. https://doi.org/10.1002/stc.2282

APPENDIX A: EXPRESSION FOR BENDING MOMENT AND SHEAR FORCE DUE TO ACCELERATING OR DECELERATING FORCE

When the distributed load on a simply supported beam is given by Equation (9) the bending moment, M, induced in the bridge girder at mid-span is,

$$\frac{M}{Sa}=f_m=\begin{cases}\left[\exp\left(-\beta L\left(\frac{1}{2}-\frac{b}{L}\right)\right)\cos\left(\beta L\left(\frac{1}{2}-\frac{b}{L}\right)\right)\right. & \\ \left.-2\exp\left(\beta L\frac{b}{L}\right)\cos\left(\beta L\frac{b}{L}\right)\right] & \text{if}\frac{b}{L}\le-\frac{1}{2}\\ \left[\exp\left(-\beta L\left(\frac{1}{2}-\frac{b}{L}\right)\right)\cos\left(\beta L\left(\frac{1}{2}-\frac{b}{L}\right)\right)\right. & \\ \left.-2\exp\left(\beta L\frac{b}{L}\right)\cos\left(\beta L\frac{b}{L}\right)\right] & \\ -\frac{h}{2a}-\frac{1}{2} & \text{if } -\frac{1}{2}\le\frac{b}{L}\le 0\\ \left[\exp\left(-\beta L\left(\frac{1}{2}-\frac{b}{L}\right)\right)\cos\left(\beta L\left(\frac{1}{2}-\frac{b}{L}\right)\right)\right. & \\ \left.-2\exp\left(\beta L\frac{b}{L}\right)\cos\left(\beta L\frac{b}{L}\right)\right] & \\ +\frac{h}{2a}+\frac{1}{2} & \text{if } 0\le\frac{b}{L}\le\frac{1}{2}\\ -\left[\exp\left(\beta L\left(\frac{1}{2}-\frac{b}{L}\right)\right)\cos\left(\beta L\left(\frac{1}{2}-\frac{b}{L}\right)\right)\right. & \\ \left.-2\exp\left(-\beta L\frac{b}{L}\right)\cos\left(\beta L\frac{b}{L}\right)\right] & \text{if}\frac{b}{L}\ge\frac{1}{2}\end{cases}, \tag{A1}$$

and the shear force, V at quarter span is,

$$\frac{2VL}{Sa}=f_s=\begin{cases}\left[L\beta\exp\left(\beta L\left(\frac{1}{4}+\frac{b}{L}\right)\right)\left\{\cos\left(\beta L\left(\frac{1}{4}+\frac{b}{L}\right)\right)\right.\right. & \\ \left.\left.-\sin\left(\beta L\left(\frac{1}{4}+\frac{b}{L}\right)\right)\right\}\right. & \\ \left.+\exp\left(-\beta L\left(\frac{1}{2}-\frac{b}{L}\right)\right)\cos\left(\beta L\left(\frac{1}{2}-\frac{b}{L}\right)\right)\right] & \text{if } \frac{b}{L}\le-\frac{1}{2}\\ \left[L\beta\exp\left(\beta L\left(\frac{1}{4}+\frac{b}{L}\right)\right)\left\{\cos\left(\beta L\left(\frac{1}{4}+\frac{b}{L}\right)\right)\right.\right. & \\ \left.\left.-\sin\left(\beta L\left(\frac{1}{4}+\frac{b}{L}\right)\right)\right\}\right. & \\ \left.+\exp\left(\beta L\left(\frac{b}{L}-\frac{1}{2}\right)\right)\cos\left(\beta L\left(\frac{1}{2}-\frac{b}{L}\right)\right)\right]-2\frac{h}{a}-2 & \text{if } -\frac{1}{2}\le\frac{b}{L}\le 0\\ -\left[L\beta\exp\left(-\beta L\left(\frac{1}{4}+\frac{b}{L}\right)\right)\left\{\cos\left(\beta L\left(\frac{1}{4}+\frac{b}{L}\right)\right)\right.\right. & \\ \left.\left.-\sin\left(\beta L\left(\frac{1}{4}+\frac{b}{L}\right)\right)\right\}\right. & \\ \left.+\exp\left(\beta L\left(\frac{1}{2}-\frac{b}{L}\right)\right)\cos\left(\beta L\left(\frac{1}{2}-\frac{b}{L}\right)\right)\right]-2\frac{h}{a}-2 & \text{if } 0\le\frac{b}{L}\le\frac{1}{2}\\ -\left[L\beta\exp\left(-\beta L\left(\frac{1}{4}+\frac{b}{L}\right)\right)\left\{\cos\left(\beta L\left(\frac{1}{4}+\frac{b}{L}\right)\right)\right.\right. & \\ \left.\left.-\sin\left(\beta L\left(\frac{1}{4}+\frac{b}{L}\right)\right)\right\}\right. & \\ \left.+\exp\left(\beta L\left(\frac{1}{2}-\frac{b}{L}\right)\right)\cos\left(\beta L\left(\frac{1}{2}-\frac{b}{L}\right)\right)\right] & \text{if } \frac{b}{L}\ge\frac{1}{2}\end{cases}. \tag{A2}$$

where, d is the distance between the centroid of the girder and the centroid of the rail and the other symbols are as explained in Section 3.2.1.

APPENDIX B: WHEEL LOADS ESTIMATED

The wheel loads estimated using the methods explained in Sections 3.1 and 3.1 for the passenger train that traversed the bridge on August 4, 2014 at 8:30 is given in Table B1. In Table B1, ASM, and SSM refer to axial strain based method and shear strain based method respectively. The locomotive front and rear bogies are represented as LF and LR, respectively. Similarly, the front and rear bogies of wagons are represented as WF and WR; and the number succeeding it representing the number of the wagon from the locomotive.

The wheel loads estimated using the methods explained in Sections 3.1 and 3.1 for the passenger train that traversed the bridge on March 23, 2014 at 10:50 is given in Table B2. The abbreviations used in the table are similar to that explained for Table B2.

TABLE B1 Loads estimated (tonnes) by both the methods for the passenger train on August 4, 2014 at 8:30 (ASM and SSM refer to axial strain based method and shear strain based method respectively; LF and LR represent the locomotive front and rear bogies respectively; WF and WR represent the wagon front and rear bogies; and the number succeeding it represents the number of the wagon from the locomotive)

Method	**LF1**	**LR1**	**WF1**	**WR1**	**WF2**	**WR2**	**WF3**	**WR3**	**WF4**
ASM	32.4	28.8	9.9	10.9	10.7	10.8	10.6	11.0	11.1
SSM	29.4	26.9	9.0	9.1	10.3	9.3	9.9	9.5	10.2
Method	**WR4**	**WF5**	**WR5**	**WF6**	**WR6**	**WF7**	**WR7**	**WF8**	**WR8**
ASM	10.8	10.6	10.8	10.2	10.6	9.7	11.3	10.0	10.4
SSM	9.4	9.9	9.7	9.7	8.8	9.2	9.8	9.6	8.5
Method	**WF9**	**WR9**	**WF10**	**WR10**	**WF11**	**WR11**	**WF12**	**WR12**	**WF13**
ASM	8.9	9.9	9.7	10.7	10.2	11.4	10.0	12.2	10.1
SSM	8.6	8.3	9.4	9.5	10.0	9.7	10.1	10.8	9.9
Method	**WR13**	**WF14**	**WR14**	**WF15**	**WR15**	**WF16**	**WR16**	**WF17**	**WR17**
ASM	11.9	12.2	14.3	10.6	12.7	10.3	11.0	8.1	9.4
SSM	10.4	11.8	12.7	10.1	10.8	10.0	10.1	8.0	8.44

TABLE B2 Loads estimated (tonnes) by both the methods for the freight train on March 23, 2014 at 10:50 (ASM and SSM refer to axial strain based method and shear strain based method respectively; LF and LR represent the locomotive front and rear bogies respectively; and WF and WR represent the wagon front and rear bogies; and the number succeeding it represents the number of the wagon from the locomotive)

Method	**LF1**	**LR1**	**LF2**	**LR2**	**WF1**	**WR1**	**WF2**	**WR2**	**WF3**	**WR3**	**WF4**	**WR4**
ASM	28.52	28.75	28.88	24.64	11.34	11.34	18.93	18.93	16.15	16.15	16.21	16.21
SSM	29.39	30.84	30.40	32.31	10.26	10.26	19.85	19.85	20.96	20.96	19.04	19.04
Method	**WF5**	**WR5**	**WF6**	**WR6**	**WF7**	**WR7**	**WF8**	**WR8**	**WF9**	**WR9**	**WF10**	**WR10**
ASM	16.67	16.67	17.11	17.11	16.77	16.77	17.70	17.70	16.46	16.46	17.70	17.70
SSM	19.97	19.97	20.75	20.75	19.33	19.33	19.90	19.90	18.82	18.82	20.53	20.53
Method	**WF11**	**WR11**	**WF12**	**WR12**	**WF13**	**WR13**	**WF14**	**WR14**	**WF15**	**WR15**	**WF16**	**WR16**
ASM	17.12	17.12	15.82	15.82	16.80	16.80	16.62	16.62	16.63	16.63	17.01	17.01
SSM	19.77	19.77	20.29	20.29	17.35	17.35	18.66	18.66	20.24	20.24	16.87	16.87
Method	**WF17**	**WR17**	**WF18**	**WR18**	**WF19**	**WR19**	**WF20**	**WR20**	**WF21**	**WR21**	**WF22**	**WR22**
ASM	16.16	16.16	17.16	17.16	16.59	16.59	17.53	17.53	16.30	16.30	17.80	17.80
SSM	19.61	19.61	18.81	18.81	19.27	19.27	18.82	18.82	19.21	19.21	19.90	19.90
Method	**WF23**	**WR23**	**WF24**	**WR24**	**WF25**	**WR25**	**WF26**	**WR26**	**WF27**	**WR27**	**WF28**	**WR28**
ASM	17.27	17.27	18.65	18.65	17.14	17.14	17.93	17.93	17.96	17.96	17.20	17.20
SSM	18.85	18.85	21.53	21.53	20.24	20.24	19.47	19.47	20.32	20.32	21.29	21.29
Method	**WF29**	**WR29**	**WF30**	**WR30**	**WF31**	**WR31**	**WF32**	**WR32**	**WF33**	**WR33**	**WF34**	**WR34**
ASM	17.48	17.48	17.29	17.29	17.98	17.98	17.59	17.59	17.24	17.24	17.44	17.44
SSM	18.76	18.76	20.29	20.29	19.74	19.74	21.33	21.33	20.15	20.15	19.83	19.83
Method	**WF35**	**WR35**	**WF36**	**WR36**	**WF37**	**WR37**	**WF38**	**WR38**	**WF39**	**WR39**	**WF40**	**WR40**
ASM	16.68	16.68	18.82	18.82	17.02	17.02	17.73	17.73	17.57	17.57	17.53	17.53
SSM	20.57	20.57	18.69	18.69	20.23	20.23	19.91	19.91	19.70	19.70	19.49	19.49
Method	**WF41**	**WR41**	**WF42**	**WR42**	**WF43**	**WR43**	**WF44**	**WR44**	**WF45**	**WR45**	**WF46**	**WR46**
ASM	17.90	17.90	19.17	19.17	18.24	18.24	18.33	18.33	17.34	17.34	18.11	18.11
SSM	21.25	21.25	19.54	19.54	19.77	19.77	21.04	21.04	17.94	17.94	21.78	21.78
Method	**WF47**	**WR47**	**WF48**	**WR48**	**WF49**	**WR49**	**WF50**	**WR50**	**WF51**	**WR51**	**WF52**	**WR52**
ASM	18.83	18.83	17.66	17.66	17.22	17.22	18.09	18.09	17.36	17.36	3.83	3.83
SSM	19.82	19.82	20.30	20.30	19.42	19.42	20.00	20.00	19.74	19.74	4.48	4.48